

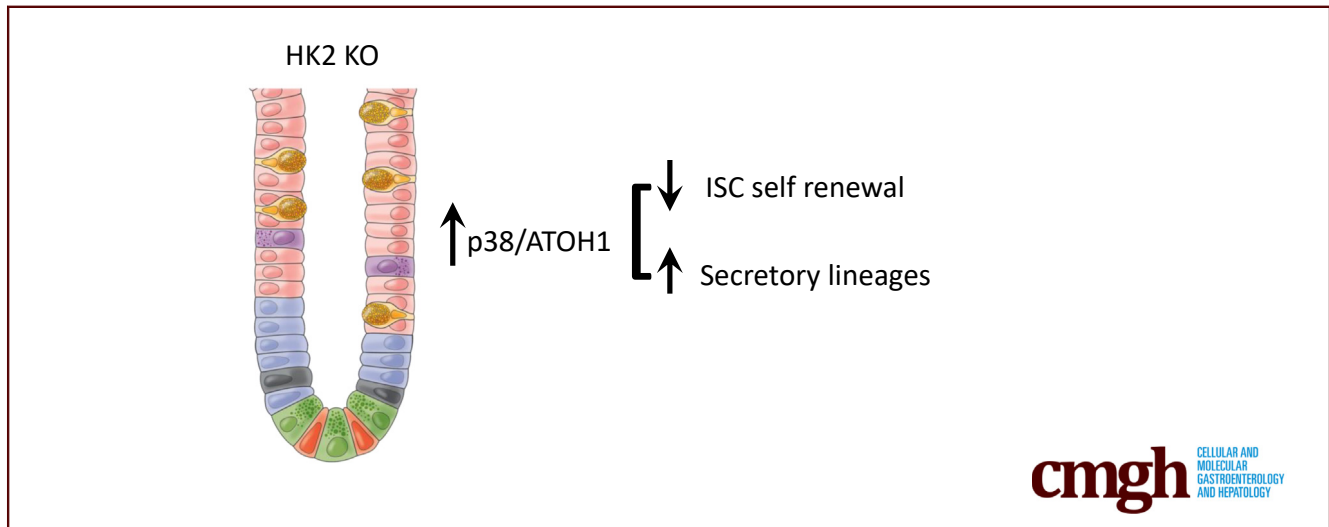
ORIGINAL RESEARCH

Glycolytic Regulation of Intestinal Stem Cell Self-Renewal and Differentiation



Chang Li,¹ Yuning Zhou,¹ Ruozheng Wei,¹ Dana L. Napier,¹ Tomoko Sengoku,¹ Michael C. Alstott,¹ Jinpeng Liu,¹ Chi Wang,¹ Yekaterina Y. Zaytseva,^{1,2} Heidi L. Weiss,¹ Qingding Wang,^{1,3} and B. Mark Evers^{1,3}

¹Markey Cancer Center, University of Kentucky, Lexington, Kentucky; ²Department of Toxicology and Cancer Biology, University of Kentucky, Lexington, Kentucky; and ³Department of Surgery, University of Kentucky, Lexington, Kentucky



SUMMARY

Our findings demonstrate that glycolytic activity is necessary to maintain intestinal stem cell (ISC) self-renewal and that limiting glycolysis contributes to the generation of secretory lineages from ISCs. The inability to fine-tune glycolysis in ISCs subsequently disturbs the balance between self-renewal and differentiation.

BACKGROUND AND AIMS: The intestinal mucosa undergoes a continual process of proliferation, differentiation, and apoptosis. An imbalance in this highly regimented process within the intestinal crypts is associated with several intestinal pathologies. Although metabolic changes are known to play a pivotal role in cell proliferation and differentiation, how glycolysis contributes to intestinal epithelial homeostasis remains to be defined.

METHODS: Small intestines were harvested from mice with specific hexokinase 2 (*HK2*) deletion in the intestinal epithelium or *LGR5*⁺ stem cells. Glycolysis was measured using the Seahorse XFe96 analyzer. Expression of phospho-p38 mitogen-activated protein kinase, the transcription factor atonal

homolog 1, and intestinal cell differentiation markers lysozyme, mucin 2, and chromogranin A were determined by Western blot, quantitative real-time reverse transcription polymerase chain reaction, or immunofluorescence, and immunohistochemistry staining.

RESULTS: *HK2* is a target gene of Wnt signaling in intestinal epithelium. *HK2* knockout or inhibition of glycolysis resulted in increased numbers of Paneth, goblet, and enteroendocrine cells and decreased intestinal stem cell self-renewal. Mechanistically, *HK2* knockout resulted in activation of p38 mitogen-activated protein kinase and increased expression of *ATO1*; inhibition of p38 mitogen-activated protein kinase signaling attenuated the phenotypes induced by *HK2* knockout in intestinal organoids. *HK2* knockout significantly decreased glycolysis and lactate production in intestinal organoids; supplementation of lactate or pyruvate reversed the phenotypes induced by *HK2* knockout.

CONCLUSIONS: Our results show that *HK2* regulates intestinal stem cell self-renewal and differentiation through p38 mitogen-activated protein kinase/atonal homolog 1 signaling pathway. Our findings demonstrate an essential role for glycolysis in maintenance of intestinal stem cell function. (*Cell Mol Gastroenterol Hepatol* 2023;15:931–947; <https://doi.org/10.1016/j.jcmgh.2022.12.012>)

Keywords: Intestinal Stem Cells; Glycolysis; HK2; Metabolism.

The mammalian intestinal mucosa undergoes a dynamic process of constant and rapid renewal characterized by active proliferation of crypt-based stem cells localized near the base of the crypts.¹ As these cells progress up the crypt-villus axis, there is cessation of proliferation and subsequent differentiation into 1 of 4 main primary cell types (enterocytes, goblet cells, Paneth cells, and enteroendocrine cells).^{1,2} An imbalance in this highly regimented and orderly process is associated with common intestinal pathologies, including colorectal cancer and inflammatory bowel disease (IBD), which cause significant morbidity and mortality.^{3,4}

Metabolic changes play a pivotal role in regulating cell proliferation and differentiation.⁵ Normal tissue- and cell-specific metabolic pathways are tightly regulated during differentiation and perform unique functions in specific cell contexts.⁵ Compared with their differentiated progeny, stem cells are characterized by distinct metabolic activities with a higher glycolysis and a lower fraction of oxidative phosphorylation (OXPHOS).⁶ Moreover, Paneth cells provide lactate to support the high OXPHOS and mitochondrial activity in *LGR5*⁺ intestinal stem cells (ISCs) of small intestinal organoids.⁷ Previously, we showed that intestinal cell differentiation is associated with decreased glycolysis.⁸ However, it is not entirely known if and how the altered glycolysis affects the fate of discrete subtypes of intestinal epithelial cells and their molecular characteristics during differentiation, and this represents a major gap in the understanding of intestinal homeostasis. Elucidation of the effects of altered metabolism that governs development, survival, and function of discrete intestinal cell types may provide more suitable and selective therapeutic approaches for improving intestinal regeneration and function in patients.

Hexokinases (HKs) are critical enzymes regulating the irreversible bioconversion of glucose to glucose-6-phosphate in glucose metabolism. Four major HK isoforms, denoted as HK1, HK2, HK3, and HK4 (also known as glucokinase or GCK), are expressed in mammalian tissues.⁹ Clinical and animal studies indicate that HK2 likely plays a critical role in the pathogenesis of diseases, such as ischemic injury and cancers.¹⁰⁻¹² In the intestine, HK2, a major contributor to increased glycolysis,¹³ is predominantly expressed by intestinal epithelial cells.¹⁴ Loss of epithelial HK2 protects against acute intestinal inflammation¹⁴; however, its overall function in ISC proliferation and differentiation remains poorly understood. Considering the importance of glycolysis in intestinal disorders, it is critical to better understand the exact roles that glycolysis and HK2 play in ISC function. Here, we provide evidence that HK2 plays an important role in regulation of ISC self-renewal and differentiation. Complete ablation of *HK2* is embryonically lethal.¹⁵ Therefore, we used *HK2*^{fl/fl}; *Villin-creERT2* and *HK2*^{fl/fl}; *LGR5-EGFP-IRES-creERT2* conditional intestinal knockout (KO) models and found that HK2 contributes to the maintenance of ISC function.


Results

HK2 Is Regulated by Wnt Signaling in Intestinal Cells

To determine the role of glycolysis in the intestine, we first determined the differential expression of *HKs* in intestinal cells. Analysis of single-cell transcriptome data of small intestine epithelial cells from Haber et al.¹⁶ demonstrated that *HK2* was mainly expressed in goblet, enteroendocrine, and stem cells (Figure 1A). In contrast, *HK1* and *HK4* (*GCK*) are mainly expressed in Tuft and endocrine cells, respectively, whereas *HK3* is less expressed in intestinal epithelium. These results suggest that *HK2* is the main isoform expressed in the intestinal epithelium. Ubiquitously expressed *HK2* was noted in crypts as shown by in situ hybridization (ISH) (Figure 1B). Moreover, dual ISH confirmed the concordance between *LGR5* and *HK2* expression in the intestine (Figure 1C). These data suggested a possible role for *HK2* in the maintenance of goblet, enteroendocrine, and *LGR5*⁺ ISCs in the small bowel. To further analyze the concordance of *LGR5* and *HK2* expression, we isolated intestinal crypts from *LGR5-EGFP-IRES-creERT2* knock-in mice by flow cytometry of intestinal cells with high green fluorescent protein (GFP) expression (*LGR5-GFP*^{high} ISCs) and the more differentiated *GFP*^{low} progenitors.¹⁷ Similar to the expression pattern of ISC markers *LGR5* and *ASCL2*, *HK2* was mainly expressed in *LGR5-GFP*^{high} ISCs (Figure 1D).

Because Wnt signaling plays a critical role in ISC self-renewal and differentiation, we next used the organoid culture system to determine whether *HK2* expression was regulated by Wnt signaling. Treatment with CHIR99021, a Wnt agonist,¹⁸ increased mRNA expression of *HK2* and *AXIN2*, a well-known Wnt target gene (Figure 1E). In contrast, treatment with the tankyrase inhibitor, XAV939, which antagonizes Wnt,¹⁸ dose-dependently decreased *HK2* and *AXIN2* mRNA expression (Figure 1F). We next determined whether loss of *APC* could increase *HK2* expression because *APC* mutation leads to hyperactivation of Wnt signaling.¹⁹ We isolated the crypts from *APC*^{fl/fl} (wild-type [WT]) or *APC*^{fl/fl}; *Villin-creERT2* mice and cultured for growing organoids. The organoids were treated with 4-hydroxytamoxifen (4-OHT) to induce the deletion of *APC*. As shown in Figure 1G, *APC* deletion (*APC* KO) resulted in increased *HK2* and *AXIN2* mRNA expression. Similarly, the

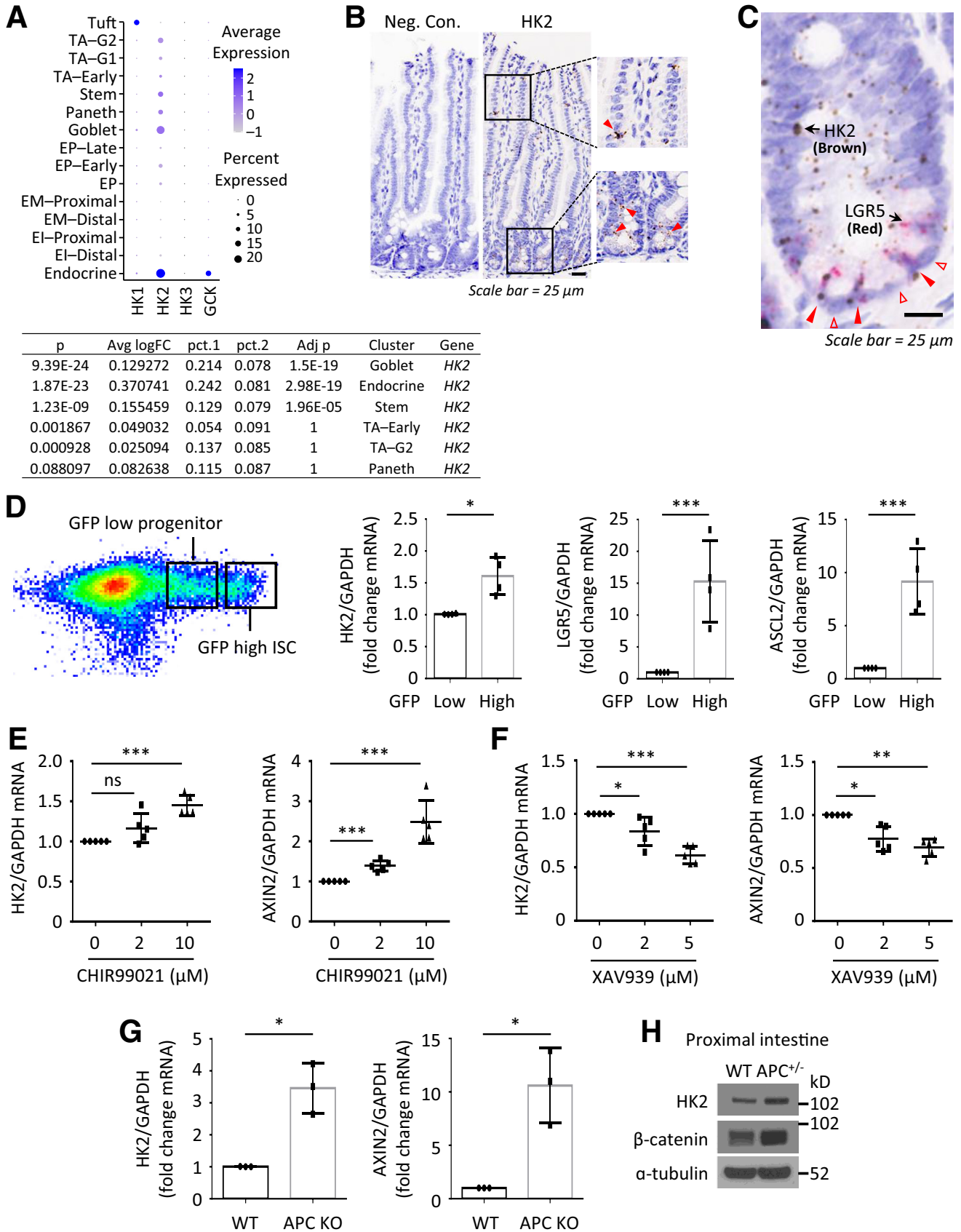
Abbreviations used in this paper: 2-DG, 2-deoxyglucose; 4-OHT, 4-hydroxytamoxifen; ANG4, angiogenin 4; CGA, chromogranin A; DEFA, defensin; GFP, green fluorescent protein; HK2, hexokinase 2; IBD, inflammatory bowel disease; IF, immunofluorescence; ISC, intestinal stem cell; ISH, in situ hybridization; KO, knockout; LYZ, lysozyme; MAPK, mitogen-activated protein kinase; MUC2, mucin 2; OXPHOS, oxidative phosphorylation; PBS, phosphate-buffered saline; qPCR, quantitative real-time reverse transcription polymerase chain reaction; TAM, tamoxifen; WT, wild-type.

 Most current article

© 2023 The Authors. Published by Elsevier Inc. on behalf of the AGA Institute. This is an open access article under the CC BY-NC-ND license (<http://creativecommons.org/licenses/by-nc-nd/4.0/>).

2352-345X

<https://doi.org/10.1016/j.jcmgh.2022.12.012>



increased HK2 expression was further demonstrated in the intestinal epithelium isolated from *APC^{f/+}; Villin-cre* mice (Figure 1H). These results demonstrate that *HK2*, which is mainly expressed in ISCs, is regulated by Wnt signaling, suggesting that *HK2* may play a critical role in ISC self-renewal and differentiation.

HK2 Loss Increases Intestinal Cell Differentiation

We have shown that intestinal cell differentiation is associated with decreased glycolysis.⁸ To determine the role of *HK2* in the intestine, we crossed *HK2^{f/f}* mice to *Villin-creERT2* mice and engineered *HK2^{f/f}; Villin-creERT2*, a conditional intestinal KO model that disrupts *HK2* in all intestinal epithelial cell types on tamoxifen (TAM) administration. We administered 5 doses of TAM starting at postnatal day 45 to *HK2* KO (*HK2^{f/f}; Villin-creERT2*) and WT control mice (*HK2^{f/f}*); 5 days post-TAM, intestinal tissues were harvested for analysis (Figure 2A).

Administration of TAM specifically reduced *HK2* expression in the intestinal epithelium as noted by Western blot (Figure 2B), quantitative real-time reverse transcription polymerase chain reaction (qPCR) (Figure 2C), and ISH (Figure 2D). Intestinal *HK2* loss resulted in an increase in the number of goblet cells in the small bowel as noted by mucin 2 (*MUC2*) (Figure 2E and F) and Alcian blue staining (Figure 2G and H). Staining the intestinal sections from *HK2* KO mice for lysozyme (*LYZ*) revealed an obvious increase in Paneth cells (Figure 2I–K). Moreover, the number of *LYZ*⁺ cells in the upper crypts of *HK2* KO mice was also significantly increased (Figure 2I and K). Furthermore, increased chromogranin A (*CGA*)⁺ enteroendocrine cells were found in the small intestine of *HK2* KO mice (Figure 2L and M). Thus, our studies indicate that *HK2* KO results in ISC differentiation toward the secretory lineage. *HK2* KO did not alter body weight (Figure 3A), colon and small intestinal length (Figure 3B and C), morphology of the small intestine and villus length or crypt depth (Figure 3D), and the proliferation as determined by Brdu incorporation (Figure 3E and F).

Loss of HK2 Represses Intestinal Stemness

To further investigate the role of *HK2* in regulating ISC maintenance, we generated a stem cell-specific *HK2* KO mouse model *HK2^{f/f}; LGR5-EGFP-IRES-creERT2* mouse,

where the *LGR5* knock-in allele permits the isolation of *LGR5-GFP^{high}* containing ISCs by flow cytometry and the deletion of *HK2* in the *GFP^{high}* subset of ISCs on TAM administration (Figure 4A). This model is often used to quantify *GFP^{high}* containing ISCs and *GFP^{low}* progenitors.^{20,21} We ablated *HK2* in 6-week-old *LGR5-GFP* mice (Figure 4A) and intestinal cells with high GFP expression (*Lgr5-GFP^{high}* ISCs) and lower GFP expression (*Lgr5-GFP^{low}* progenitors) were gated. *HK2* loss decreased the frequency of *LGR5-GFP^{high}* containing ISCs by 50% (Figure 4B).

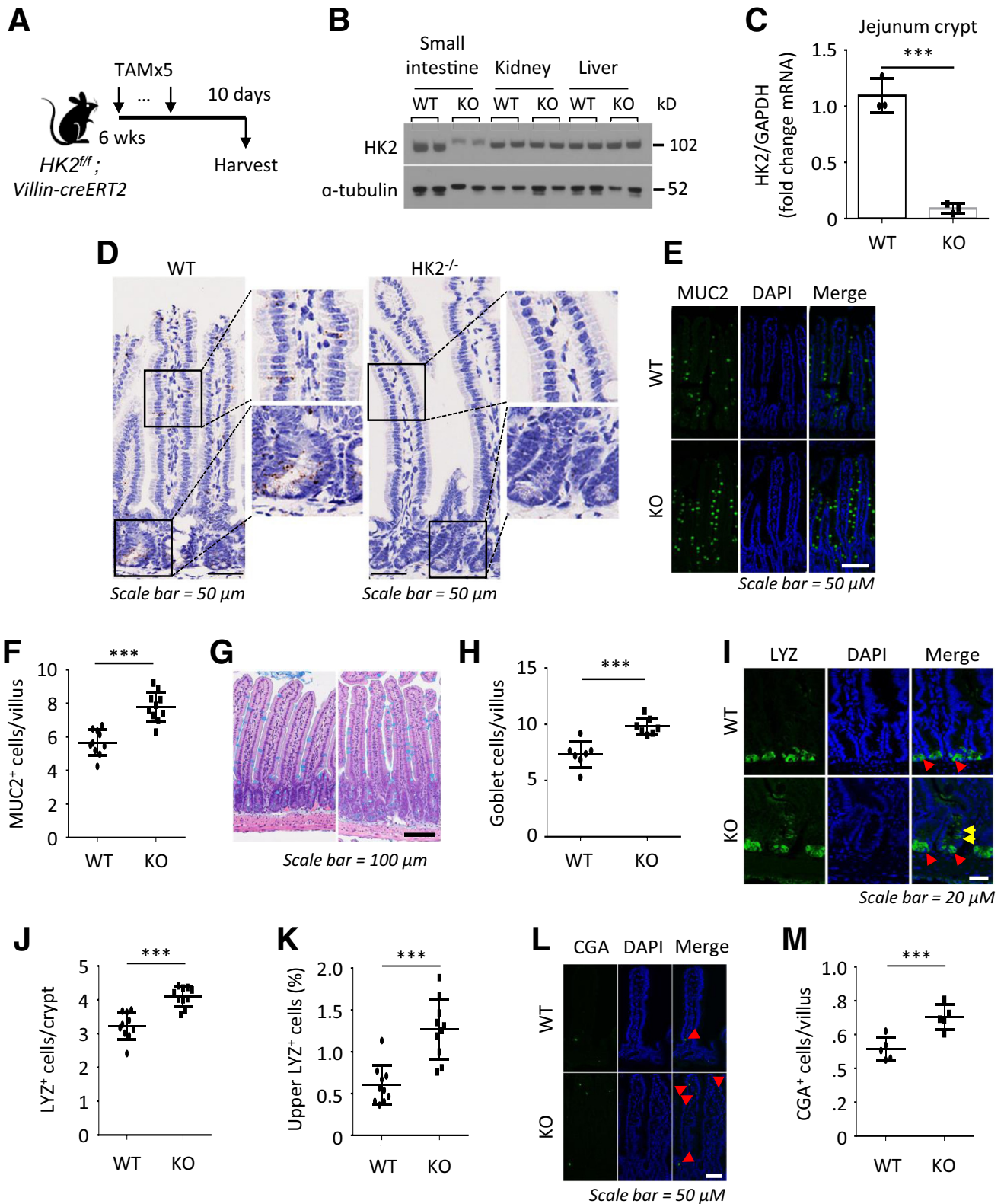
Intestinal organoids, generated from whole crypts, represent an established model system for studying intestinal development and maintenance. We next determined the effects of *HK2* loss on growth of intestinal organoids. The activity of ISCs was assessed based on their ability to drive the formation of organoids.^{22,23} Crypts were isolated from WT control or *HK2^{f/f}; Villin-creERT2* mice at Day 5 after the last TAM injection and cultured to grow organoids. Organoids cultured from WT control mice continued to grow and underwent extensive budding. By contrast, *HK2* deletion led to a decrease in crypt organoid-forming capacity (Figure 4C) and the formation of small organoids (Figure 4D and E) with no effect on cell death (Figure 4F). As an assessment of the renewal capacity of organoid-forming cells,²⁴ we next tested whether *HK2* was required for the formation of secondary organoids. Interestingly, *HK2*-deficient organoids generated secondary organoids at much lower rates than *HK2* WT control organoids (Figure 4G). Our results suggest that *HK2* loss represses ISC self-renewal (ie, fewer ISC numbers with less organoid-forming potential).

To further determine the role of *HK2* in intestinal cell differentiation, crypts isolated from WT control or *HK2^{f/f}; Villin-creERT2* mice were cultured, and the organoids were treated with 4-OHT to induce *HK2* deletion (Figure 5A). Treatment with 4-OHT results in the decreased expression of *HK2* (Figure 5B), formation of small organoids, and decreased number of lobes per organoid (Figure 5C–E), another indicator of stem cell function.²⁵ As observed in mouse intestine, *HK2* deletion in organoids increased levels of many secretory cell markers, such as *MUC2*, *LYZ*, and *CGA* and *GCG* (Figure 5F–G). Paneth cells contain distinct

Figure 1. (See previous page). *HK2* is a target gene of Wnt signaling in intestinal cells. (A) Expression of *HKs* was analyzed by scRNA sequencing. “pct.1” is the percentage of *HK2* expressing cells in the selected cell type (eg, Goblet). The “pct.2” is the percentage of *HK2* expressing cells in the rest of cells (eg, all non-Goblet cells). El, enterocyte immature; EM, enterocyte mature; EP, enterocyte progenitor. TA, transit amplifying; G1, G1/S cell-cycle phase; G2, G2/M cell-cycle phase. (B) RNA-scope brown staining of *HK2* in intestinal crypts from WT mice. (C) *HK2* is mainly expressed in *LGR5*-positive cells but not in Paneth cells. RNA scope duplex staining of *HK2* (brown) with *LGR5* (red) in WT jejunum crypts. (D) *HK2* is more highly expressed in *GFP^{high}* cells. Small intestine crypts from the *LGR5-EGFP-IRES-creERT2* mice were harvested and digested with Trypsin LE for 30 minutes to obtain single cells. *GFP^{high}* and *GFP^{low}* cells were isolated by fluorescence-activated cell sorting. Expression of *ASCL2*, *LGR5*, and *HK2* was determined by qPCR. Data represent mean ± SD (n = 4 mice). (E and F) Small intestinal crypts from jejunum of WT mice were harvested and seeded in 24-well plates. Organoids were treated with either vehicle control (DMSO) or Wnt agonist CHIR99021 (D) or Wnt antagonist XAV939 (E) for 3 days. Total RNA was extracted and expression of *HK2* and *AXIN2* was analyzed by qPCR (n = 5 mice). (G) Small intestinal crypts from *APC^{f/f}* and *APC^{f/f}; Villin-creERT2* mice were harvested and seeded into 24-well plates and cultured for 24 hours followed by treatment with 4-OHT (1 mM) for 24 hours to induce knockout of *APC* expression. Four days after removing 4-OHT, total RNA was extracted and expression of *HK2* and *AXIN2* was determined by qPCR (n = 3 mice). (H) Western blotting analysis of protein expression in WT and *APC^{f/+}; Villin-cre* mice. Intestinal mucosa from 3-month-old mice was collected for analysis. **P* < .05; ***P* < .01; ****P* < .005.

cytoplasmic granules for exocytosis of antimicrobial peptides, such as LYZ, defensins (DEFA), and angiogenin 4 (ANG4). We next determined whether *HK2* KO affects

expression of *ANG4* and *DEFA alpha 5 (DEFA5)*. Consistent with the increased number of Paneth cells, increased expression of *ANG4* and *DEFA5* was noted in *HK2* KO mice



compared with WT mice (Figure 5F), further demonstrating that HK2 deficiency promotes Paneth cell differentiation. HK2 deletion in organoids increased number of secretory cell lineages was also demonstrated by IF staining (Figure 5H). Together, these data demonstrate that loss of HK2 in the small bowel not only represses ISC self-renewal but also shifts early differentiation within the crypt toward the secretory lineage (ie, greater numbers of Paneth, goblet, and enteroendocrine cells).

HK2 regulates ISC self-renewal and differentiation through the regulation of p38 mitogen-activated protein kinase (MAPK)/ATOH1 pathway

To determine the mechanisms involved in the regulation of ISC function by HK2/glycolysis, we used glycolysis inhibitor 2-deoxyglucose (2-DG). Similar to HK2 KO, treatment of organoids with 2-DG repressed organoid growth and increased differentiation (Figure 6A–C). Interestingly, we found that 2-DG treatment resulted in an increase in ATOH1 mRNA expression (Figure 7A). Because ATOH1 is required for differentiation of secretory cell lineages in the small bowel,²⁶ our results suggest that glycolysis regulates secretory lineage generation through ATOH1. p38 MAPK alpha is required for secretory differentiation.²⁷ Moreover, 2-DG has been shown to induce energy stress through the inhibition of glycolysis and subsequent activation of the p38 MAPK pathway in mouse embryonic fibroblast cells.²⁸ We next determined whether inhibition of glycolysis using 2-DG affects the activation of p38 MAPK in intestinal cells. As shown in Figure 7B, treatment of intestinal cells with 2-DG resulted in the increased activation of p38 MAPK as noted by the increased phosphorylation of p38 MAPK. Consistent with results using 2-DG, we found that HK2 KO increased ATOH1 mRNA expression (Figure 7C) and p38 MAPK phosphorylation in HK2 KO organoids (Figure 7D). Therefore, these results demonstrate that HK2 regulates secretory cell differentiation through increased ATOH1 expression and activation of p38 MAPK.

Because inhibition of p38 MAPK has been shown to repress ATOH1 expression in intestinal epithelial cells,²⁷ we next tested whether activation of p38 MAPK mediates the phenotypes induced by HK2 KO. Organoids derived from HK2 KO mice showed decreased growth, which was rescued by addition of SB202190, a selective p38 MAPK inhibitor (Figure 7E and F). Moreover, HK2 KO increased expression of LYZ, MUC2, ATOH1, and CGA; this increase was blocked by inhibition of p38 MAPK (Figure 7G and H). Importantly,

these results suggest that activation of p38 MAPK is required for HK2 KO repression of ISC self-renewal and promotion of ISC differentiation.

Lactate Reverses the Phenotypes Induced by HK2 Knockout

To further study the HK2/glycolytic activity involved in HK2-dependent regulation of ISC function, we next assessed glycolysis by measuring extracellular acidification rate in crypt organoids as described.²⁹ As shown in Figure 8A, HK2 KO results in decreased extracellular acidification rate, which is associated with decreased glycolytic capacity. Consistent with these results, decreased lactate production was noted in HK2 KO organoids compared with HK2 WT organoids (Figure 8B), indicating impairment of glycolytic activity in organoids with HK2 deletion. We next tested whether supplementation of lactate could rescue the repressed organoid size and increased secretory lineages in the HK2 KO organoids. As shown in Figure 8C and D, supplementation of lactate partially restored the organoid size in the 4-OHT-induced HK2 KO organoids. We further observed that lactate attenuates or blocks the increased secretory lineage markers and ATOH1 expression in the HK2-deficient organoids (Figure 8E). Moreover, addition of lactate attenuates the increased p38 MAPK phosphorylation induced by HK2 KO in organoids (Figure 8F). Similar results were noted in organoids treated with pyruvate, another glycolytic product. Pyruvate attenuates or blocks the increased secretory lineage markers and ATOH1 expression in the HK2-deficient organoids (Figure 9). These results show that lactate/pyruvate treatment rescues the phenotypic consequences of HK2 deficiency in intestinal cells and further implicates a crucial role for HK2/glycolysis in promoting ISC self-renewal and repressing ISC differentiation.

Discussion

Metabolic changes are known to play a pivotal role in cell proliferation and differentiation.⁵ However, it is not entirely known if and how the altered glycolysis affects the fate of discrete subtypes of intestinal epithelial cells and their molecular characteristics during differentiation. The present study identifies HK2 as a critical enzyme for the maintenance of ISC homeostasis. Deleting HK2 in LGR5⁺ ISCs repressed ISC stemness, and HK2 KO or inhibition of glycolysis increased the number of Paneth, goblet, and enteroendocrine cells and repressed ISC self-renewal. Moreover, HK2 regulates ISC self-

Figure 2. (See previous page). **HK2 loss increases differentiation of secretory cells.** (A) Schematic of HK2^{fl/fl}; Villin-creERT2 mouse model, including the timeline of TAM injection and tissue collection. (B) Western blotting analysis of HK2 expression in small intestine mucosa, kidney, and liver tissues from WT and HK2 KO mice. (C) Expression of HK2 in WT and HK2 KO jejunum crypts was determined by qPCR (n = 3 mice). (D) The expression of HK2 in WT and HK2 KO mice was analyzed by ISH. (E) IF staining of jejunum from WT and HK2 KO mice with DAPI and MUC2. (F) Quantification of MUC2⁺ goblet cells in villus (n = 10 mice; at least 20 villi were counted from each mouse). (G) AB staining of jejunum of WT and HK2 KO mice. (H) Quantification of AB⁺ goblet cell in villi (at least 20 villi counted per mouse; n = 7 mice). (I) IF staining of jejunum from WT and HK2 KO mice with DAPI and LYZ. (J) Quantification of LYZ⁺ Paneth cells in crypt (n = 10 mice; at least 20 crypts were counted from each mouse). (K) Quantification of number of LYZ⁺ cells in the upper crypts based on LYZ IF staining (n = 10 mice; at least 20 crypts were counted from each mouse). (L) IF staining of jejunum from WT and HK2 KO mice with DAPI and CGA. (M) Quantification of CGA⁺ EE cell in crypts (n = 5 mice; at least 20 villi were counted from each mouse). ***P < .005.

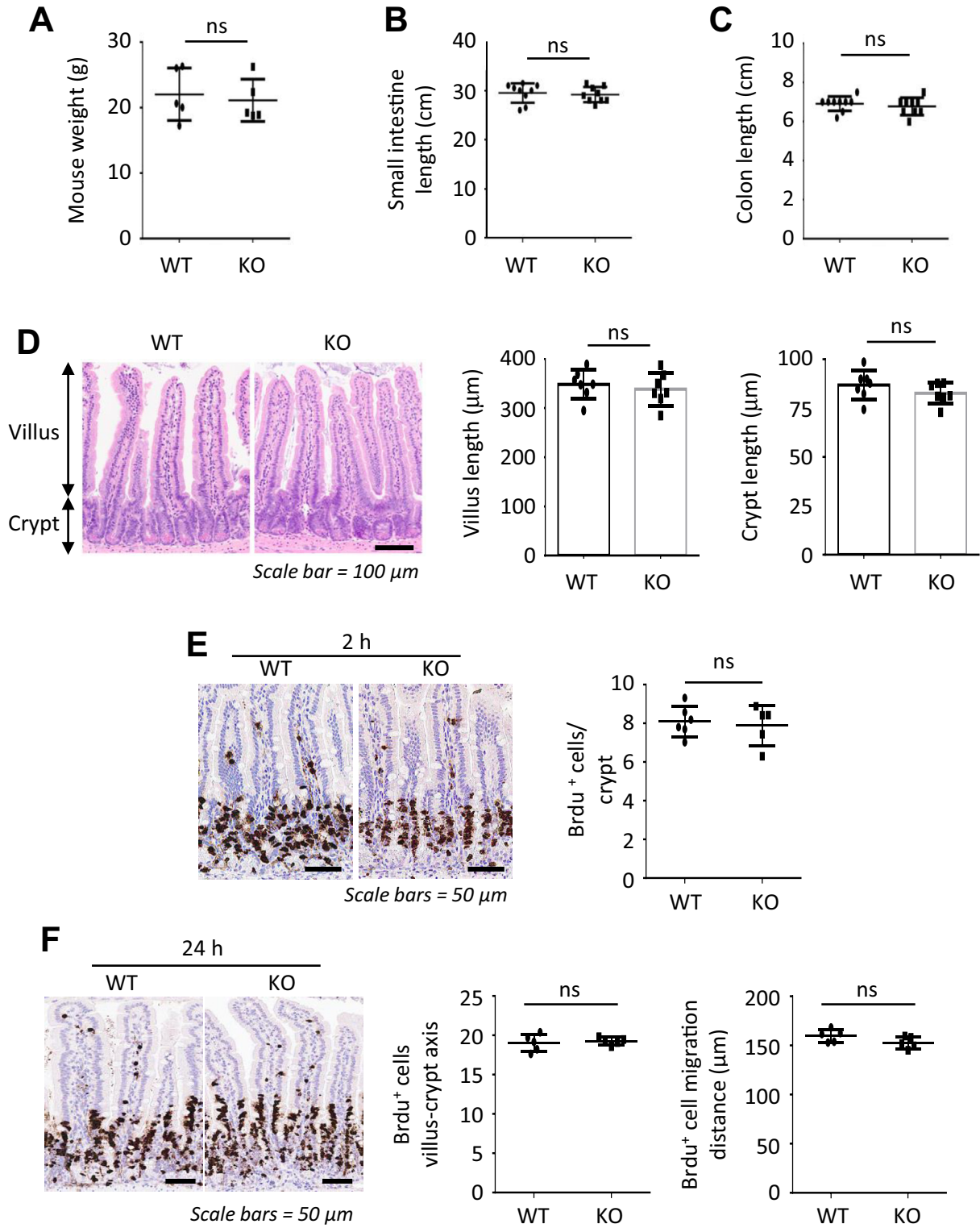


Figure 3. Effects of HK2 loss on the intestinal architecture. (A) Body weight from WT and *HK2* KO mice (n = 5 mice). (B) The length of small intestine was determined in WT and *HK2* KO mice (n = 9 mice). (C) The length of colon was determined in WT and *HK2* KO mice (n = 9 mice). (D) Hematoxylin-eosin staining of jejunum slices from WT and *HK2* KO mice; the length of the villi and crypts was analyzed (at least 20 villi or crypts measured per mouse; n = 7 mice). (E and F) BrdU staining of jejunum of WT and *HK2* KO mice and quantification of BrdU⁺ cell in villi and villus-crypt axis (at least 20 crypts or villus-crypt axis counted per mouse; n = 56 mice), 2 (E) or 24 (F) hours after BrdU administration.

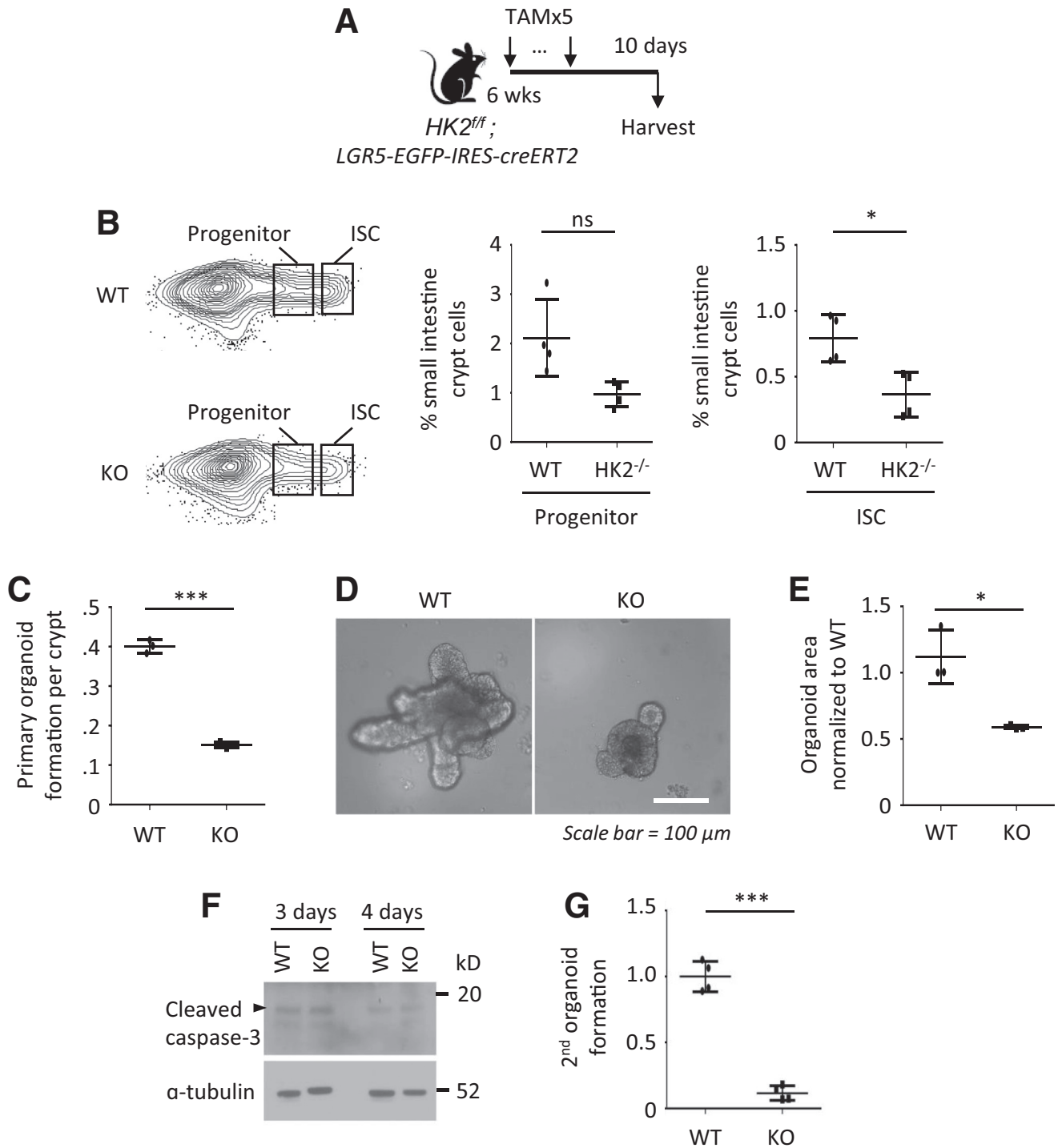
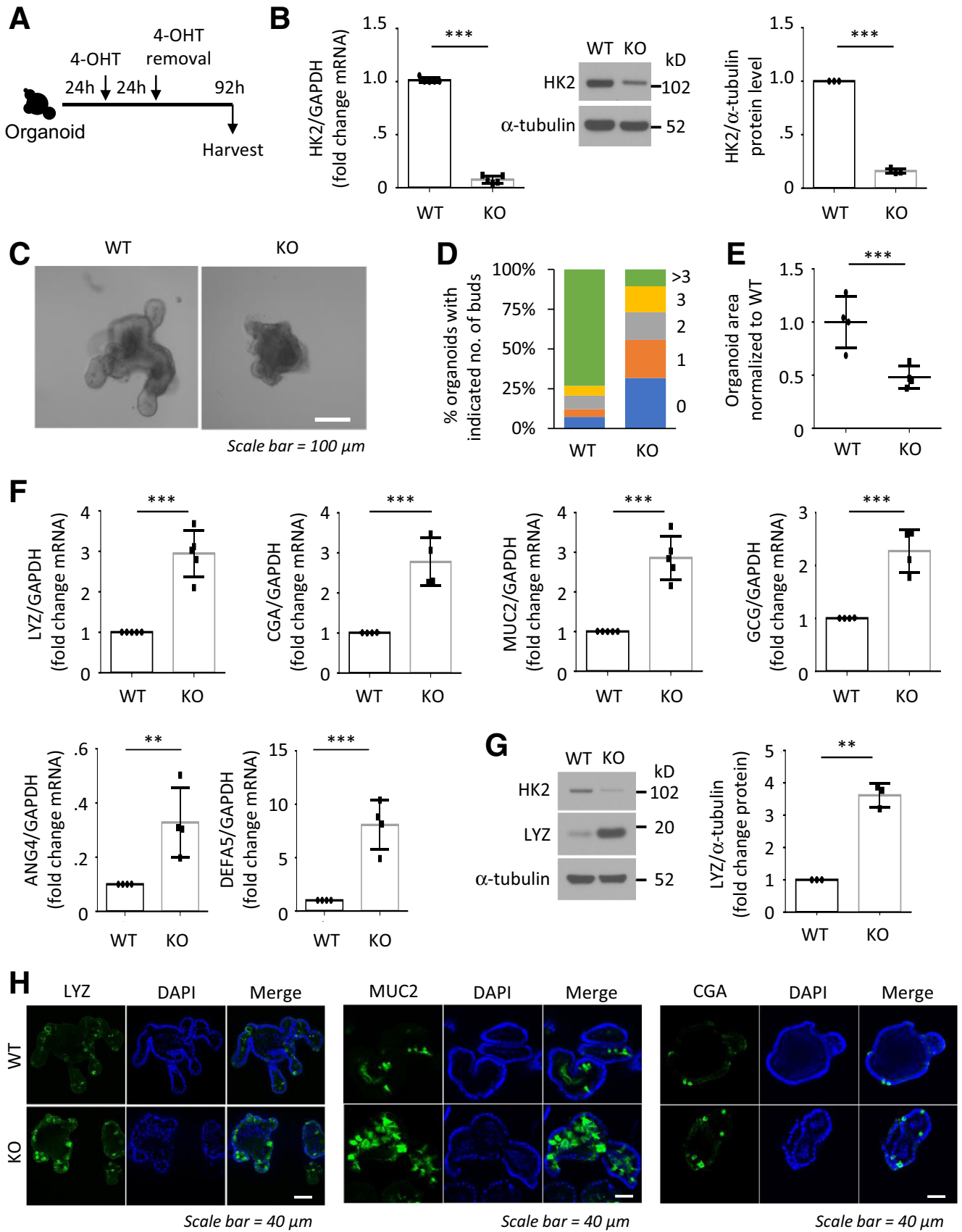


Figure 4. Loss of *HK2* represses intestinal stemness. (A) Schematic of the mouse model, including the timeline of TAM injection and tissue collection. (B) Frequency of EpCAM⁺/PI⁻/Lgr5-GFP^{high} ISCs and Lgr5-GFP^{low} progenitors in crypt cells from WT and *HK2* KO mice by flow cytometry (n = 4 mice). (C–E) WT and *HK2^{ff}; Villin-creERT2* mice were injected with 5 dosages of TAM, and small intestine crypts were collected. Organoid-forming assay is shown in C (n = 3 mice). The picture of organoids from WT and *HK2* KO mice is shown in D. Quantification of the organoid area from WT and *HK2* KO mice is shown in E (at least 30 organoids were measured per mouse; n = 3 mice per group). (F) The crypts from *HK2^{ff}* and *HK2^{ff}; Villin-creERT2* mice were treated with 4-OHT for 24 hours to induce KO of *HK2*. Organoids were harvested 3 or 4 days after removal of 4-OHT, and cleaved caspase-3 was determined by Western blot. (G) *HK2* KO decreases the secondary colony formation. The number of organoids per well (n = 4) were counted and expressed as a fold change compared with WT. **P* < .05; ****P* < .005.



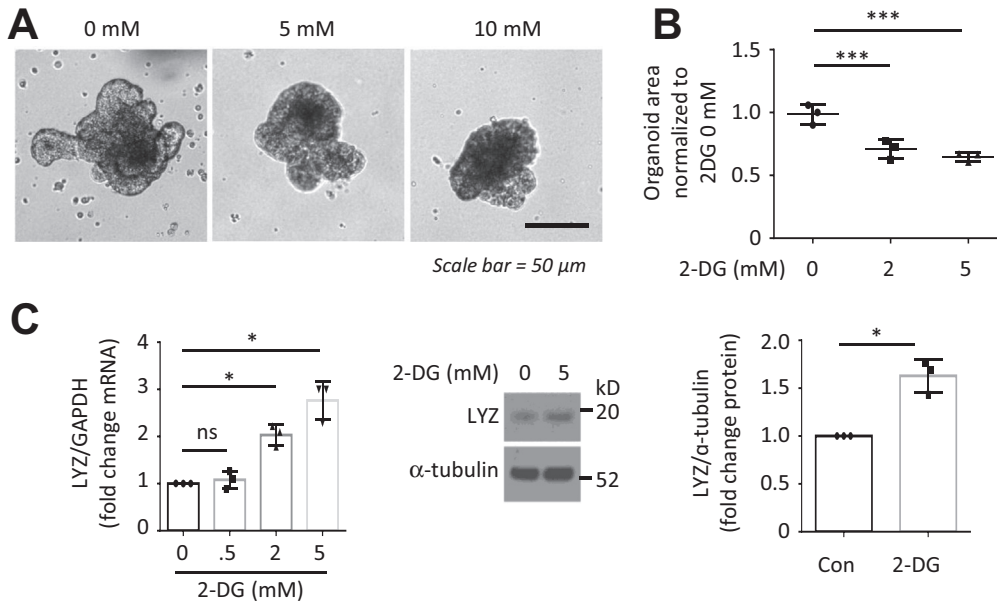


Figure 6. Treatment with glycolysis inhibitor 2-DG repressed organoid growth. Small intestinal organoids from WT mice were treated with 2-DG for 3 days. (A) Morphology of organoids. (B) Quantification of the organoid size from control and 2-DG treatment (at least 30 organoids were measured per mouse; $n = 3$ mice). (C) The expression of LYZ mRNA was detected by qPCR and Western blot ($n = 3$ mice). * $P < .05$; *** $P < .005$.

renewal and differentiation through the regulation of the p38 MAPK/ATOH1 signaling pathway. Importantly, these findings demonstrate that fine-tuned glycolysis is critical for the maintenance of ISC function.

Our findings identify *HK2* as a target gene of Wnt signaling in the intestinal epithelium. Activation of Wnt/ β -catenin has been shown to promote glycolysis.^{30,31} Our results suggest that Wnt regulates glycolysis, at least in part, through regulation of *HK2* expression. Moreover, Wnt signaling plays a critical role in ISC self-renewal and differentiation. The balance between self-renewal and differentiation in ISCs is regulated by Wnt signaling. We found that *HK2* is mainly expressed in LGR5-GFP^{high} ISCs compared with the more differentiated GFP^{low} progenitors. In addition, our findings show that *HK2* contributes to ISC self-renewal and *HK2* KO promotes ISC differentiation into Paneth cells, goblet cells, and enteroendocrine cells. Therefore, we show that *HK2*, as a target gene of Wnt signaling, mediates the function of Wnt signaling in the regulation of ISC self-renewal and differentiation.

Immature intestinal epithelial cells, a product of the ISCs, differentiate into absorptive or secretory cells. We found that loss of *HK2* increased the expression of *ATOH1*, which is required for secretory lineage generation in the intestine,²⁶ implying that *HK2* regulates secretory cell differentiation through the regulation of *ATOH1* expression. We also found

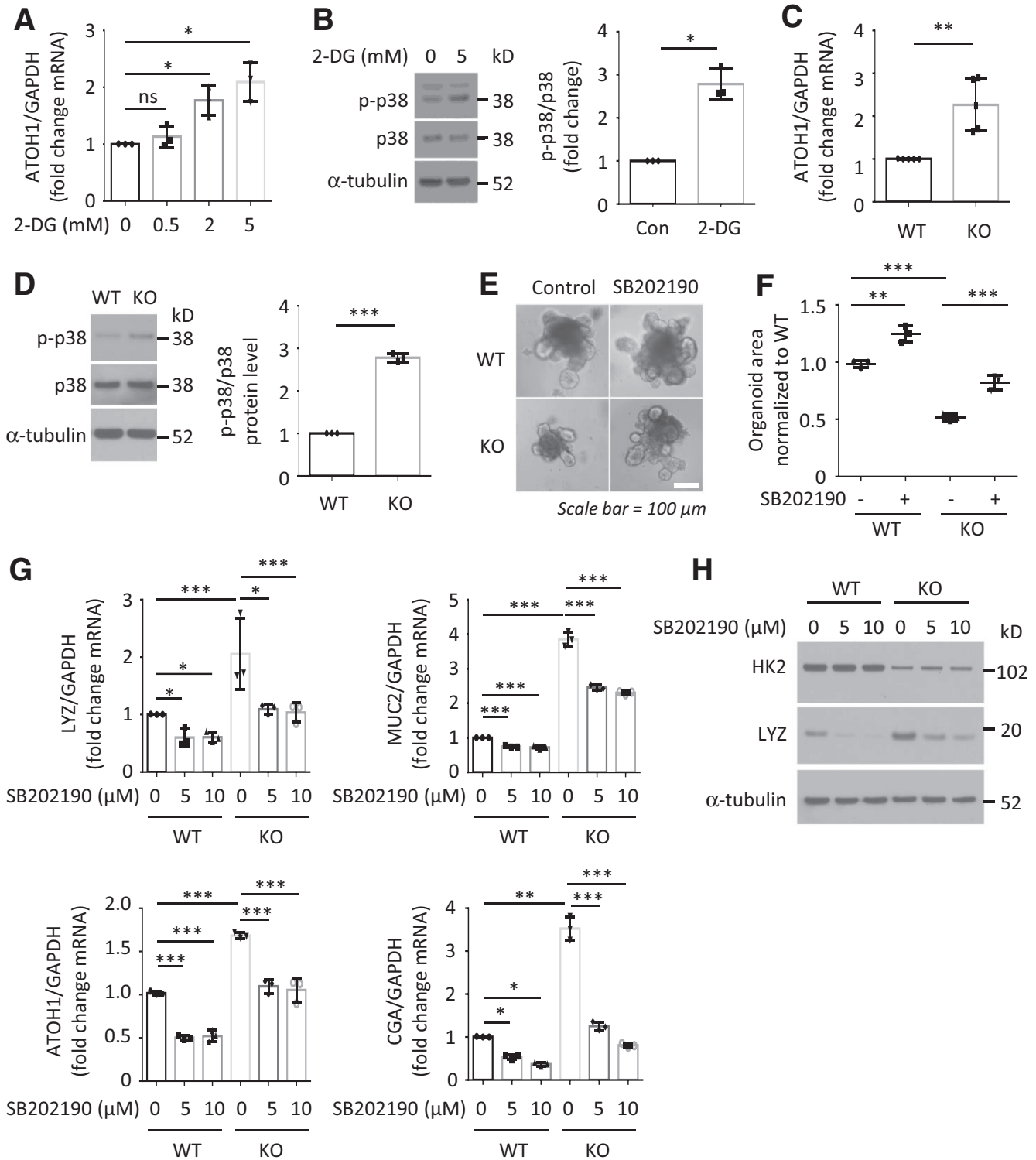
that *HK2* regulated *ATOH1* through p38 MAPK signaling. Activation of p38 MAPK contributes to aging associated ISC exhaustion.³² p38 MAPK inhibition is required for long-term maintenance of human intestinal organoids.³³ In addition, intestine-specific p38a KO mice showed a decreased secretory differentiation in intestine.²⁷ Our findings identify p38 MAPK and *ATOH1* as downstream signaling molecules of *HK2* and reveal a critical role for *HK2*/p38 MAPK/*ATOH1* pathway in the regulation of secretory lineage generation in the intestine.

Importantly, we demonstrate that *HK2* deficiency promotes ISC differentiation resulting in increased secretory lineage cells. Recently, it has been shown that deletion of *HK2*, which is highly expressed in intestinal epithelium from patients with IBD, protects against dextran sulfate sodium-induced acute intestinal colitis in mice.¹⁴ However, the mechanisms involved in this protection are not clear. Alterations in intestinal epithelial cell subtypes, including reduced numbers of goblet and Paneth cells, are frequently observed in inflammatory conditions.³⁴ Dysfunction of goblet and Paneth cells is often observed in patients with IBD and can contribute to disease pathogenesis.³⁵⁻³⁸ In addition, Paneth cell defects contribute to the origin of gut inflammation in models of IBD,³⁹ and Paneth cell dysfunction contributes to mucosal dysbiosis in patients with IBD and in mouse models.^{36,40,41} Mucus secreted from goblet cells serves as an important barrier to prevent pathogens

Figure 5. (See previous page). *HK2* deficiency promotes secretory cell differentiation in organoids. (A) Schematic of the organoid model, including the timeline of 4-OHT treatment and organoid collection. (B) *HK2* expression was determined by qPCR ($n = 5$ mice) and Western blot ($n = 3$ mice). (C) Representative image of WT and *HK2* KO organoids. (D) Quantification of the budding number of WT and *HK2* KO organoids (at least 30 organoids were measured per mouse). One representative result from 3 biologic independent experiments is shown. (E) Organoid size derived from indicated genotypes was quantified (at least 30 organoids were measured per mouse; $n = 4$ mice). (F) qPCR analysis for *MUC2*, *LYZ*, *ANG4*, and *DEFA5*. *CGA* and *GCG* in organoids from indicated genotypes ($n = 4-5$ mice). (G) LYZ protein expression in WT and *HK2* KO organoids determined by Western blot. LYZ signals from 3 mice were quantitated densitometrically and expressed as fold change with respect to α -tubulin. (H) IF staining of LYZ (left), *MUC2* (middle), and *CGA* (right) in WT and *HK2* KO organoids. ** $P < .01$; *** $P < .005$.

from invading the mucosa.⁴² The abnormal differentiation of goblet cells results in the deficient synthesis and secretion of mucins and thus intestinal mucosal barrier dysfunction.⁴² Our findings suggest that deletion of *HK2* may contribute to

attenuate the dextran sulfate sodium-induced acute intestinal inflammation by promoting ISC differentiation into Paneth and goblet cell lineages. Although targeted *HK2* inhibition can attenuate dextran sulfate sodium-induced acute in-



testinal inflammation, our results show that *HK2* deletion can also repress ISC self-renewal, suggesting a limitation in the consideration of targeting *HK2* as a therapeutic option for chronic inflammation.

Compared with the differentiated progeny cells, stem cells are often characterized by distinct metabolic activities with higher glycolysis and a lower fraction of mitochondrial OXPHOS.⁶ We showed that *HK2* KO in ISCs decreased ISC self-renewal. Moreover, *HK2* KO decreased glycolytic activity and lactate production in intestinal cells, whereas supplementation of lactate or pyruvate reversed these phenotypes induced by *HK2* KO. Our results demonstrate that glycolysis in ISCs is critical for the maintenance of ISC function. Our study establishes a paradigm wherein glycolysis plays a direct role in controlling ISC fate. Previously, we have shown that intestinal cell differentiation is associated with decreased glycolysis.⁸ In agreement with our findings, other investigators have shown that proliferative cells in intestinal crypt are characterized by a glycolytic metabolic phenotype, whereas differentiated intestinal epithelium maintain an OXPHOS phenotype.⁴³ Activating mitochondrial OXPHOS by substitution of glucose with galactose has shown to promote ISC differentiation.⁷ Together, these findings suggest that ISCs show a preference for glycolysis for self-renewal but shift to an OXPHOS-dependent metabolism driving differentiation.

Previously, Rodriguez-Colman et al.⁷ showed that OXPHOS in ISCs and glycolysis in Paneth cells are required to support ISC function; however, this study was limited by using only in vitro epithelial cell cultures. In addition, whether and how altered glycolysis in ISCs affects ISC self-renewal and differentiation is not known. In contrast, our study provides several lines of evidence demonstrating a critical role of glycolysis to directly promote ISC function: (1) *HK2*, a major contributor to increased glycolysis,¹³ is mainly expressed in ISC but not in Paneth cells; (2) specific deletion of *HK2* in ISCs repressed ISC stemness; and (3) inhibition of glycolysis or specific deletion of *HK2* in ISCs promotes ISC differentiation. Our results demonstrate that glycolysis in ISCs is required to support ISC function.

In conclusion, our findings demonstrate that glycolysis is necessary and sufficient to maintain ISC self-renewal and that limiting glycolysis contributes to the generation of secretory lineages from ISCs. The inability to fine-tune glycolysis in ISCs subsequently disturbs the balance

between self-renewal and differentiation. Elucidation of the effects of altered glycolysis that govern the function of discrete intestinal cell types may provide more suitable and selective therapeutic approaches for improving intestinal regeneration and function in patients.

Materials and Methods

Mouse Strains

To investigate the necessity of *HK2* in maintaining ISC functions, we obtained *HK2^{fl/fl}* mice from Dr Nissim Hay⁴⁴ (College of Medicine, University of Illinois at Chicago) and crossed them with *LGR5-EGFP-IRES-creERT2* mice (B6.129P2-*Lgr5^{tm1(cre/ERT2)Cle}/J*, Strain #008875) to generate *HK2^{fl/fl}; LGR5-EGFP-IRES-creERT2* mice. *HK2^{fl/fl}; Villin-creERT2* mice were generated by crossing *HK2^{fl/fl}* mice to *Villin-creERT2* mice (B6.Cg-Tg[Vil1-cre/ERT2]23Syr/J, Strain #020282). As control animals, we used littermate *HK2^{fl/fl}* mice, referred to as WT mice. *Apc^{15lox}* mice (B6.129P2-*Apc^{tm1Rsmi}/Rfo*), Strain #029275) were crossed with *Villin-creERT2* mice to generate *APC^{fl/fl}; Villin-creERT2* mice. *APC/Villin-cre* mouse colonies were established by mating *Villin-cre* mice (B6.Cg-Tg[Vil1-cre]1000Gum/J, Strain # 021504) with *APC* mice (C57BL/6-*Apc^{tm1Tyj}/J*, Strain #009045).

Mice were maintained on a 12 hours light/dark schedule in filter top isolators with autoclaved water under specific pathogen-free conditions and fed autoclaved standard laboratory chow ad libitum. Age- and gender-matched mice were used for all experiments. All animal procedures were conducted in accordance with National Institutes of Health guidelines and were approved by the University of Kentucky Institutional Animal Care and Use Committee.

Mouse Intestinal Crypt Isolation and Organoid Culture

Intestinal crypts and villi were isolated as previously reported.⁴⁵ Briefly, mouse small intestine was opened longitudinally, washed with ice-cold phosphate-buffered saline (PBS) to remove the luminal contents, and cut into 2- to 4-mm pieces. The intestinal fragments were incubated in ice-cold PBS containing 10 mM EDTA for 60 minutes at 4°C. Crypts were released by shaking with ice-cold PBS. Washing in ice-cold PBS was repeated until most of the crypts were released, as determined by microscopic analysis. Crypt suspensions were passed through a 70- μ m cell strainer and

Figure 7. (See previous page). *HK2* regulates ISC self-renewal and differentiation through the regulation of p38 MAPK/ATOH1 pathway. (A and B) Small intestine organoids from WT mice were treated with 2-DG for 3 days. Treatment with 2-DG increased *ATOH1* mRNA expression (A) and p38 phosphorylation (B). Phosphorylated p38 MAPK expression from 3 separate experiments was quantitated densitometrically and expressed as fold change with respect to total p38 MAPK. (C and D) Crypts from *HK2^{fl/fl}* and *HK2^{fl/fl}; Villin-creERT2* mice were treated with 4-OHT for 24 hours to induce KO of *HK2*. *HK2* KO increased the expression of *ATOH1* in organoids as noted in C (n = 5 mice). *HK2* KO increased p38 phosphorylation in intestinal organoids as shown in D. Phosphorylated p38 MAPK signals from *HK2* WT (n = 3 mice) and *HK2* KO (n = 3 mice) were quantitated densitometrically and expressed as fold change with respect to total p38 MAPK. (E–H) Crypts from *HK2^{fl/fl}* and *HK2^{fl/fl}; Villin-creERT2* mice were treated with 4-OHT for 24 hours to induce KO of *HK2*; the p38 inhibitor SB202190 was added together with 4-OHT for 24 hours and alone for an additional 4 days. Inhibition of p38 MAPK attenuated the decrease in organoid size on *HK2* KO as noted in E. Quantification of the size of organoids derived from indicated genotypes is shown in F (at least 30 organoids per mouse were measured; n = 3 mice). Inhibition of the p38 pathway attenuated the increased expression of secretory markers in *HK2* KO organoids as shown in G (n = 3 mice). Inhibition of the p38 pathway attenuated the increased LYZ protein expression in *HK2* KO organoids as shown in H. **P* < .05; ***P* < .01; ****P* < .005.

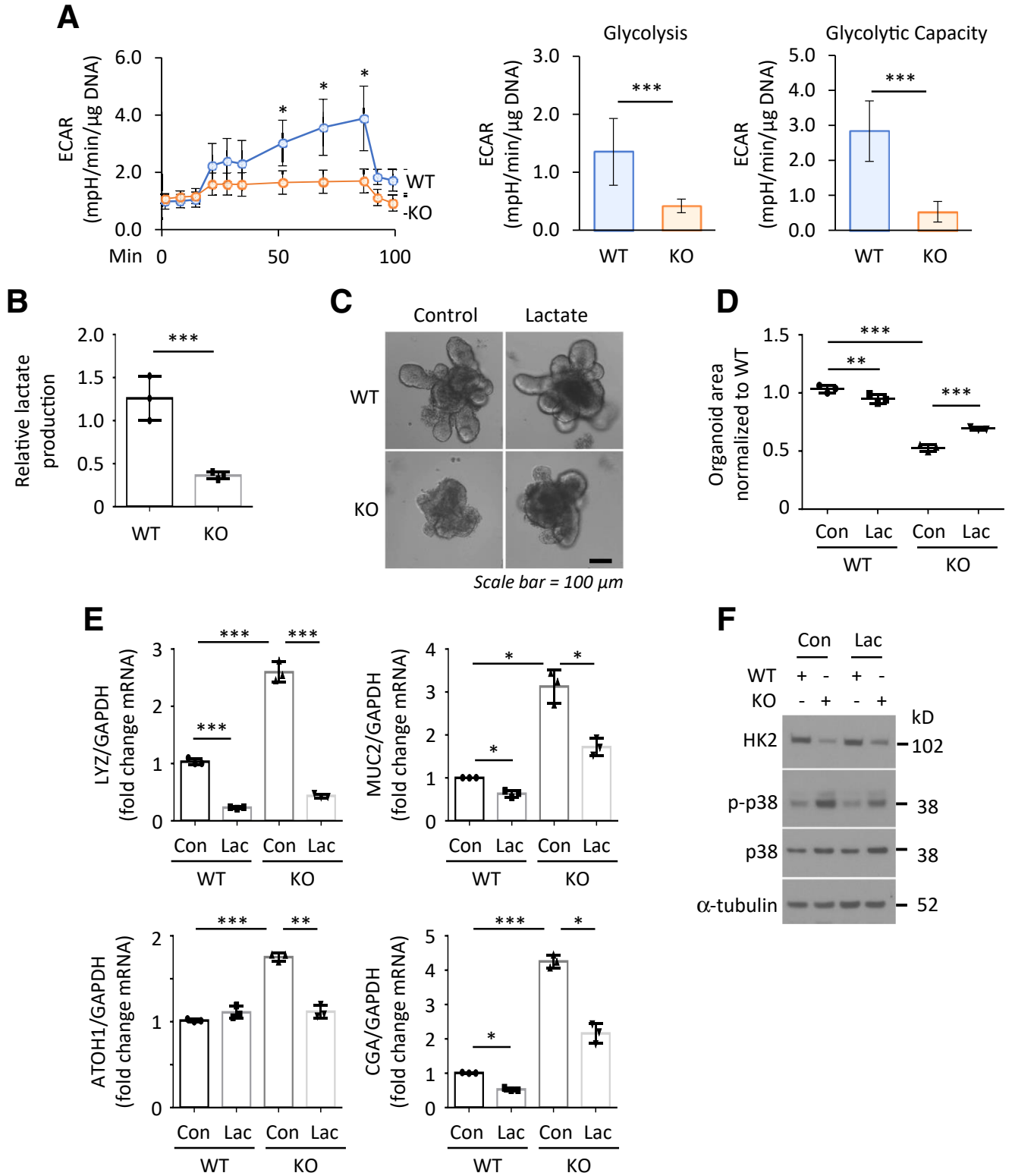


Figure 8. Lactate reverses the phenotypes induced by HK2 KO. (A) Seahorse analysis of intestinal WT and HK2 KO organoids (n = 4 wells). One representative result from 3 biologic independent experiments is shown. (B) The crypts from HK2^{fl/fl} and HK2^{fl/fl}; Villin-creERT2 mice were incubated, and organoids were treated with 4-OHT for 24 hours to induce KO of HK2. Three days after 4-OHT treatment, culture media was collected, and lactate in the media was measured and results normalized by total DNA amount (n = 3 mice). (C–F) The crypts from HK2^{fl/fl} and HK2^{fl/fl}; Villin-creERT2 mice were cultured and crypt organoids treated with 4-OHT for 24 hours to induce KO of HK2. Lactate (10 mM) was added to the medium together with 4-OHT for 24 hours and continuous treatment for an additional 4 days. Supplementation of lactate attenuated the decrease in organoid size induced by HK2 KO as shown in C. Quantification of the size of organoids derived from indicated genotypes is shown in D (at least 30 organoids were measured per mouse; n = 3 mice). Supplementation of lactate attenuated the increased expression of secretory markers in HK2 KO organoids as shown in E (n = 3 mice). Supplementation of lactate attenuated activation of p38 MAPK associated with HK2 KO as noted in the Western blot shown in F. *P < .05; **P < .01; ***P < .001.

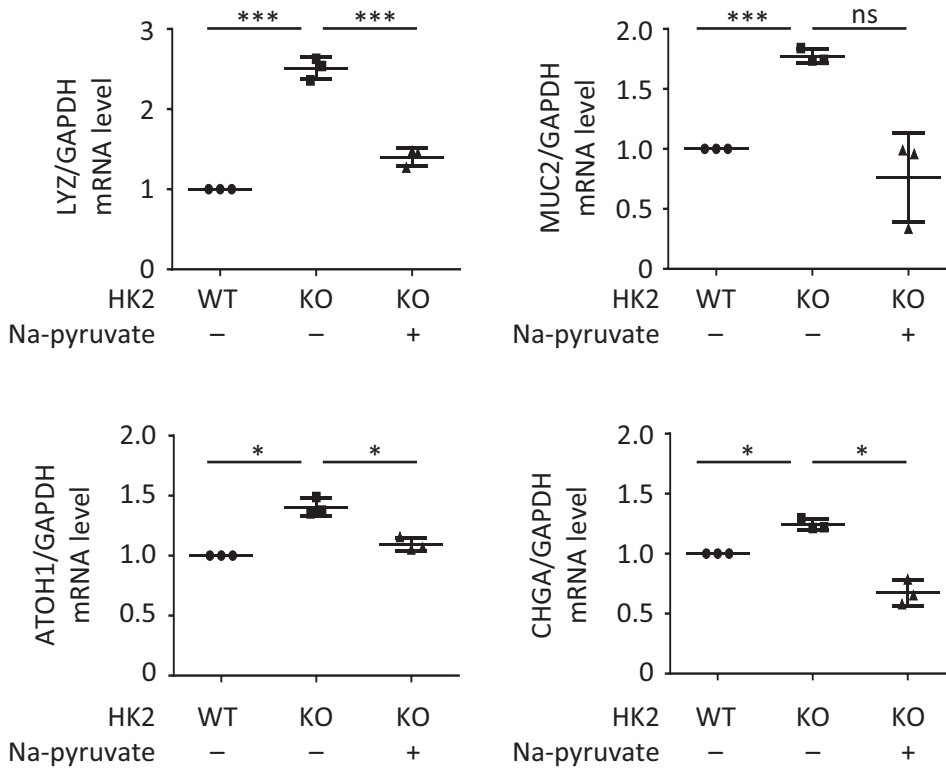


Figure 9. Pyruvate reverses the increase of secretory cell differentiation induced by *HK2* KO. The crypts from *HK2^{fl/fl}* and *HK2^{fl/fl}; Villin-creERT2* mice were cultured and crypt organoids treated with 4-OHT for 24 hours to induce KO of *HK2*. Sodium pyruvate (10 mM) was added to the medium together with 4-OHT for 24 hours and continuous treatment for an additional 4 days. qPCR analysis for *MUC2*, *LYZ*, *CGA*, and *ATOH1* mRNA expression in organoids from indicated genotypes (n = 3 mice). **P* < .05; ****P* < .005.

centrifuged at $300 \times g$ for 5 minutes. Isolated crypts were mixed with Matrigel and cultured in IntestiCult Organoid Growth Medium (Mouse, stem cell tech Catalog # 06005) as described previously.⁷ Colony-forming efficiency was calculated by plating 200 crypts and assessing organoid formation 3 days after initiation of cultures as described.²¹ The organoid area was measured as described.⁴⁶ Briefly, the surface area of organoids was measured by taking several random nonoverlapping photographs of organoids using a microscope. Photographs were analyzed using ImageJ software. Organoid perimeters for area measurements were defined manually. Measurements from *HK2* WT organoids were compared with *HK2* KO organoids to determine the relative area change. Secondary colony formation was determined as described.²⁴ Briefly, the same number of crypts from *HK2^{fl/fl}* and *HK2^{fl/fl}; Villin-creERT2* mice was cultured and treated with 4-OHT for 24 hours to induce KO of *HK2*. After removal of 4-OHT, crypt organoids were continually cultured for 4 days. Then, 1 well of organoids from WT and *HK2* KO was incubated for 2 minutes in TrypLE Express (Invitrogen) to form fragments of ~10–20 cells and then plated into 4 wells. The number of organoids recovered from each well was quantified.

Seahorse Analysis

Agilent Seahorse Analyzer was used to measure extracellular acidification rate in organoids as described.⁴⁷ Briefly, intestinal crypts from *HK2^{fl/fl}* and *HK2^{fl/fl}; Villin-creERT2* mice were seeded in 24-well plates and treated with

4-OHT for 24 hours to induce *HK2* deletion. Two days after 4-OHT treatment, the organoids were transferred to XFe96 cell culture microplates and cultured for an additional 24 hours before measurement. Extracellular acidification rate was measured on addition of glucose to induce glycolytic flux, oligomycin to induce the glycolytic reserve, and 2-DG to inhibit glycolysis. Extracellular acidification rate values per group were normalized to the total amount of DNA present in all wells of the according group.

In Situ Hybridization

ISH was carried out on the Ventana Discovery Ultra platform, using RNAScope VS Universal HRP (for singleplex) (Advanced Cell Diagnostics) or RNAScope VS Duplex Reagent (dual stain) (Advanced Cell Diagnostics) with RNAScope probes directed against Ms-HK2 and Ms-LGR5 (Advanced Cell Diagnostics). Staining conditions were optimized on the test tissue using RNAScope's Ms-PPIB probe as a positive control, and DapB probe as negative control before staining with probes of interest.

Histology

Sections from WT and *HK2* KO mice were stained with hematoxylin-eosin as described.⁴⁸ Morphology was assessed in high-quality sections containing nonfragmented villi. Villus height and crypt depth were measured with Aperio ImageScope – Pathology Slide Viewing Software (Leica Biosystems Imaging, Inc, Vista, CA) as described.⁴⁵ Briefly, crypt depth was measured as the length between the

bottom of the crypts and the crypt-villus junction; villus height was determined by the length between the crypt-villus junction and the top of the villus. At least 20 well-oriented crypts and villi were counted per mouse by a single blinded observer.

Immunofluorescence, Immunohistochemistry, and Alcian Blue Staining

Immunofluorescence (IF), immunohistochemistry, and Alcian blue staining were performed as described previously.⁴⁸ Tissues were processed for routine IF or immunohistochemistry staining using the following antibodies: rabbit anti-LYZ (Diagnostic BioSystems, Pleasanton, CA), anti-MUC2 (ThermoFisher), and anti-CGA (Santa Cruz, Dallas, TX). Negative control animals (including no primary antibody or isotype-matched mouse IgG) were used in each assessment. Alcian blue staining was performed according to standard protocol using Alcian blue pH 2.5 Stain Kit (Dako, Carpinteria, CA).

BrdU Assay

Five days after the final TAM administration, mice were injected with 100 μ L of BrdU (10 mg/mL, intraperitoneally) (BD Pharmingen) at 2 or 24 hours before sacrifice. A small section of jejunum tissues was processed for routine immunostaining. For proliferation, the percentage of BrdU-positive cells relative to total cell number per crypt or per villus-crypt axis was quantified. Migration distance was measured as the distance from the bottom of crypts to foremost BrdU positive enterocytes as described.⁴⁹

Fluorescence-Activated Cell Sorting

Crypts were harvested from the proximal jejunum (~10 cm) of *LGR5-eGFP-IRES-creERT2* mice by 60-minute incubation with ice-cold EDTA/PBS (10 mM) and filtered through a 70- μ m strainer. Crypts were dissociated by incubating with TryPLE for 20 minutes (Gibco, Waltham, MA; 12604013) at 37° C. TryPLE was stopped by adding Advanced DMEM (Gibco; 12491015) containing 10% fetal bovine serum (Gibco; 10270106) and dissociated cells were passed through a 40- μ m strainer. For EpCAM⁺ isolation, cells were stained with PI (Life Technologies) and anti-EpCAM antibody (eBioscience) and gated on GFP^{high} (stem cells) and GFP^{low} (progenitors). Cell sorting was performed on a BD fluorescence-activated cell sorting Aria II System as described.⁵⁰

Quantitative Real-Time Reverse Transcription Polymerase Chain Reaction Analysis

Total RNA was extracted and treated with DNase (Promega, Madison, WI). Synthesis of cDNA was performed using reagents in the TaqMan Reverse Transcription Reagents Kit (Applied Biosystems, Foster City, CA). TaqMan probe and primers were purchased from Applied Biosystems. qPCR was performed as described previously.⁸

Lactate Production Analysis

The crypts from *HK2^{fl/fl}* and *HK2^{fl/fl}; Villin-creERT2* mice were collected and cultured. Crypt organoids were treated

with 4-OHT for 24 hours to induce KO of *HK2*. After removal of 4-OHT, organoids were continually cultured for 2 days. Culture medium was replaced with the fresh medium 24 hours before organoid harvesting. The lactate concentration in the medium was measured using an EnzyChrom L-Lactate Assay Kit (BioAssay Systems ECLC-100). The DNA isolated from the organoids was used for normalization of lactate concentration.

Western Blot Analysis

Western blotting was performed as described.⁸ Antibodies to HK2 (Genetex), phospho-p38, p38, and α -tubulin (all from Cell Signaling) and LYZ (Diagnostic BioSystems) were used.

Reanalysis of Bulk RNA-Seq

We reanalyzed the single-cell transcriptome data of small intestine epithelial cells (EpCAM⁺, CD45⁻, TER-119⁻, and CD31⁻)¹⁶ containing 7216 cells. The Unique Molecular Identifier count matrix and cell cluster labels were retrieved from GSE92332. Unique Molecular Identifier counts were normalized by sequencing depth for each cell, multiplied by a scale factor 10,000, and then natural log transformed.⁵¹ Dot plots were used to visualize the expression of selected genes.⁵¹ Dot size represents the fraction of cells in the cluster that express the gene; color indicates the mean expression in expressing cells, relative to other clusters. Differential expression tests were carried out using FindAllMarkers function based on Wilcoxon rank sum test.⁵¹

Statistical Analysis

For in vitro experiments and in vivo studies, comparisons of HK2, LYZ⁺, MUC2⁺, and CGA⁺, extracellular acidification rate, morphology, IF, and immunohistochemistry between 2 groups were performed using 2-sample Student *t* test or analysis of variance for multiple groups with contrast statements. Adjustment in *P* values because of multiple pairwise testing between groups was performed using the Holm step-down procedure. Linear mixed models were used for in vivo studies comparing WT and *HK2* KO to account for multiple observations from multiple crypts and villi per mouse. Normality and equality of variance assumptions for study end points were assessed to determine validity of statistical tests and models. Bar graphs represent mean \pm standard deviation levels in each group. For in vitro studies, 3 replicates were used for each cell culture condition and each experiment was repeated at least 3 times. Representative data from the repeat experiments are presented. All data from animal samples with measurement of study end points were included in the analysis. All authors had access to the study data and have reviewed and approved the final manuscript.

References

1. Santos AJM, Lo YH, Mah AT, et al. The intestinal stem cell niche: homeostasis and adaptations. *Trends Cell Biol* 2018;28:1062–1078.

2. Yeung TM, Chia LA, Kosinski CM, et al. Regulation of self-renewal and differentiation by the intestinal stem cell niche. *Cell Mol Life Sci* 2011;68:2513–2523.
3. Gersemann M, Wehkamp J, Stange EF. Innate immune dysfunction in inflammatory bowel disease. *J Intern Med* 2012;271:421–428.
4. Hammoud SS, Cairns BR, Jones DA. Epigenetic regulation of colon cancer and intestinal stem cells. *Curr Opin Cell Biol* 2013;25:177–183.
5. Shyh-Chang N, Daley GQ, Cantley LC. Stem cell metabolism in tissue development and aging. *Development* 2013;140:2535–2547.
6. Wei P, Dove KK, Bensard C, et al. The force is strong with this one: metabolism (over)powers stem cell fate. *Trends Cell Biol* 2018;28:551–559.
7. Rodriguez-Colman MJ, Schewe M, Meerlo M, et al. Interplay between metabolic identities in the intestinal crypt supports stem cell function. *Nature* 2017;543:424–427.
8. Wang Q, Zhou Y, Rychahou P, et al. Ketogenesis contributes to intestinal cell differentiation. *Cell Death Differ* 2017;24:458–468.
9. Robey RB, Hay N. Mitochondrial hexokinases, novel mediators of the antiapoptotic effects of growth factors and Akt. *Oncogene* 2006;25:4683–4696.
10. Zhu W, Huang Y, Pan Q, et al. MicroRNA-98 suppress Warburg effect by targeting HK2 in colon cancer cells. *Dig Dis Sci* 2017;62:660–668.
11. Bustamante MF, Oliveira PG, Garcia-Carbonell R, et al. Hexokinase 2 as a novel selective metabolic target for rheumatoid arthritis. *Ann Rheum Dis* 2018;77:1636–1643.
12. Garcia SN, Guedes RC, Marques MM. Unlocking the potential of HK2 in cancer metabolism and therapeutics. *Curr Med Chem* 2019;26:7285–7322.
13. Roberts DJ, Miyamoto S. Hexokinase II integrates energy metabolism and cellular protection: Akt on mitochondria and TORC1 to autophagy. *Cell Death Differ* 2015;22:248–257.
14. Hinrichsen F, Hamm J, Westermann M, et al. Microbial regulation of hexokinase 2 links mitochondrial metabolism and cell death in colitis. *Cell Metab* 2021;33:2355–2366.
15. Heikkinen S, Pietilä M, Halmekytö M, et al. Hexokinase II-deficient mice. Prenatal death of homozygotes without disturbances in glucose tolerance in heterozygotes. *J Biol Chem* 1999;274:22517–22523.
16. Haber AL, Biton M, Rogel N, et al. A single-cell survey of the small intestinal epithelium. *Nature* 2017;551:333–339.
17. Yilmaz OH, Katajisto P, Lamming DW, et al. mTORC1 in the Paneth cell niche couples intestinal stem-cell function to calorie intake. *Nature* 2012;486:490–495.
18. Telias M, Ben-Yosef D. Pharmacological manipulation of Wnt/ β -catenin signaling pathway in human neural precursor cells alters their differentiation potential and neuronal yield. *Front Mol Neurosci* 2021;14:680018.
19. van Lidth de Jeude JF, Meijer BJ, Wielenga MCB, et al. Induction of endoplasmic reticulum stress by deletion of Grp78 depletes Apc mutant intestinal epithelial stem cells. *Oncogene* 2017;36:3397–3405.
20. Cheng CW, Biton M, Haber AL, et al. Ketone body signaling mediates intestinal stem cell homeostasis and adaptation to diet. *Cell* 2019;178:1115–1131.
21. Mihaylova MM, Cheng CW, Cao AQ, et al. Fasting activates fatty acid oxidation to enhance intestinal stem cell function during homeostasis and aging. *Cell Stem Cell* 2018;22:769–778.
22. Li XX, Zhang HS, Xu YM, et al. Knockdown of IRE1 α inhibits colonic tumorigenesis through decreasing β -catenin and IRE1 α targeting suppresses colon cancer cells. *Oncogene* 2017;36:6738–6746.
23. Llado V, Nakanishi Y, Duran A, et al. Repression of intestinal stem cell function and tumorigenesis through direct phosphorylation of β -catenin and Yap by PKC ζ . *Cell Rep* 2015;10:740–754.
24. Stine RR, Sakers AP, TeSlaa T, et al. PRDM16 maintains homeostasis of the intestinal epithelium by controlling region-specific metabolism. *Cell Stem Cell* 2019;25:830–845.
25. Nalapareddy K, Nattamai KJ, Kumar RS, et al. Canonical Wnt signaling ameliorates aging of intestinal stem cells. *Cell Rep* 2017;18:2608–2621.
26. Yang Q, Bermingham NA, Finegold MJ, et al. Requirement of Math1 for secretory cell lineage commitment in the mouse intestine. *Science* 2001;294:2155–2158.
27. Otsuka M, Kang YJ, Ren J, et al. Distinct effects of p38 α deletion in myeloid lineage and gut epithelia in mouse models of inflammatory bowel disease. *Gastroenterology* 2010;138:1255–1265.
28. Zheng M, Wang YH, Wu XN, et al. Inactivation of Rheb by PRAK-mediated phosphorylation is essential for energy-depletion-induced suppression of mTORC1. *Nat Cell Biol* 2011;13:263–272.
29. Bas T, Augenlicht LH. Real time analysis of metabolic profile in ex vivo mouse intestinal crypt organoid cultures. *J Vis Exp* 2014;93:e52026.
30. Pate KT, Stringari C, Sprowl-Tanio S, et al. Wnt signaling directs a metabolic program of glycolysis and angiogenesis in colon cancer. *EMBO J* 2014;33:1454–1473.
31. Kawada K, Toda K, Sakai Y. Targeting metabolic reprogramming in KRAS-driven cancers. *Int J Clin Oncol* 2017;22:651–659.
32. He D, Wu H, Xiang J, et al. Gut stem cell aging is driven by mTORC1 via a p38 MAPK-p53 pathway. *Nat Commun* 2020;11:37.
33. Sato T, Stange DE, Ferrante M, et al. Long-term expansion of epithelial organoids from human colon, adenoma, adenocarcinoma, and Barrett's epithelium. *Gastroenterology* 2011;141:1762–1772.
34. Jäger S, Stange EF, Wehkamp J. Inflammatory bowel disease: an impaired barrier disease. *Langenbecks Arch Surg* 2013;398:1–12.
35. Adolph TE, Tomczak MF, Niederreiter L, et al. Paneth cells as a site of origin for intestinal inflammation. *Nature* 2013;503:272–276.
36. Liu TC, Gurram B, Baldrige MT, et al. Paneth cell defects in Crohn's disease patients promote dysbiosis. *JCI Insight* 2016;1:e86907.
37. Velcich A, Yang W, Heyer J, et al. Colorectal cancer in mice genetically deficient in the mucin Muc2. *Science* 2002;295:1726–1729.

38. McGuckin MA, Eri RD, Das I, et al. Intestinal secretory cell ER stress and inflammation. *Biochem Soc Trans* 2011;39:1081–1085.
39. Liu TC, Kern JT, Jain U, et al. Western diet induces Paneth cell defects through microbiome alterations and farnesoid X receptor and type I interferon activation. *Cell Host Microbe* 2021;29:988–1001.
40. Gulati AS, Shanahan MT, Arthur JC, et al. Mouse background strain profoundly influences Paneth cell function and intestinal microbial composition. *PLoS One* 2012;7:e32403.
41. Salzman NH, Hung K, Haribhai D, et al. Enteric defensins are essential regulators of intestinal microbial ecology. *Nat Immunol* 2010;11:76–83.
42. Yang S, Yu M. Role of Goblet cells in intestinal barrier and mucosal immunity. *J Inflamm Res* 2021;14:3171–3183.
43. Stringari C, Edwards RA, Pate KT, et al. Metabolic trajectory of cellular differentiation in small intestine by Phasor Fluorescence Lifetime Microscopy of NADH. *Sci Rep* 2012;2:568.
44. Patra KC, Wang Q, Bhaskar PT, et al. Hexokinase 2 is required for tumor initiation and maintenance and its systemic deletion is therapeutic in mouse models of cancer. *Cancer Cell* 2013;24:213–228.
45. Li C, Zhou Y, Rychahou P, et al. SIRT2 contributes to the regulation of intestinal cell proliferation and differentiation. *Cell Mol Gastroenterol Hepatol* 2020;10:43–57.
46. Sorrentino G, Perino A, Yildiz E, et al. Bile acids signal via TGR5 to activate intestinal stem cells and epithelial regeneration. *Gastroenterology* 2020;159:956–968.
47. Ludikhuijze MC, Meerlo M, Gallego MP, et al. Mitochondria define intestinal stem cell differentiation downstream of a FOXO/Notch axis. *Cell Metab* 2020;32:889–900.
48. Zhou Y, Rychahou P, Wang Q, et al. TSC2/mTORC1 signaling controls Paneth and goblet cell differentiation in the intestinal epithelium. *Cell Death Dis* 2015;6:e1631.
49. Sun X, Yang Q, Rogers CJ, et al. AMPK improves gut epithelial differentiation and barrier function via regulating Cdx2 expression. *Cell Death Differ* 2017;24:819–831.
50. Zwiggelaar RT, Lindholm HT, Fossli M, et al. LSD1 represses a neonatal/reparative gene program in adult intestinal epithelium. *Sci Adv* 2020;6:eabc0367.
51. Stuart T, Butler A, Hoffman P, et al. Comprehensive integration of single-cell data. *Cell* 2019;177:1888–1902.

Received March 25, 2022. Accepted December 20, 2022.

Correspondence

Address correspondence to: B. Mark Evers, MD, Markey Cancer Center, University of Kentucky, 800 Rose Street, H181 UK Chandler Hospital, Lexington, Kentucky 40536-0293. e-mail: mark.evers@uky.edu; or Qingding Wang, PhD, Markey Cancer Center, University of Kentucky, 760 Press Avenue, HKRB Room 321, Lexington, Kentucky 40536-0679. e-mail: qingding.wang@uky.edu.

Acknowledgements

The authors thank Dr Nissim Hay for providing *HK2^{eff}* mice; Donna Gilbreath for manuscript preparation; and the Biospecimen Procurement and Translational Pathology Shared Resource Facility, the Flow Cytometry & Immune Monitoring Shared Resource Facility, Redox Metabolism Shared Resource Facility, and the Biostatistics and Bioinformatics Shared Resource Facility of the University of Kentucky Markey Cancer Center (supported by National Cancer Institute grant P30 CA177558, to BME).

CRedit Authorship Contributions

Chang Li, PhD (Formal analysis: Equal; Investigation: Equal)
 Yuning Zhou, MD (Formal analysis: Equal; Investigation: Equal)
 Ruozheng Wei, PhD (Investigation: Equal)
 Dana L. Napier, PhD (Investigation: Equal)
 Tomoko Sengoku, PhD (Investigation: Equal)
 Michael C. Alstott, PhD (Investigation: Equal)
 Jinpeng Liu, PhD (Formal analysis: Equal)
 Chi Wang, PhD (Formal analysis: Equal; Methodology: Equal)
 Yekaterina Y. Zaytseva, PhD (Investigation: Equal)
 Heidi L. Weiss, PhD (Formal analysis: Equal; Methodology: Equal)
 Qingding Wang, PhD (Conceptualization: Equal; Formal analysis: Equal; Methodology: Equal; Visualization: Equal; Writing – original draft: Equal)
 B. Mark Evers, MD (Conceptualization: Equal; Formal analysis: Equal; Funding acquisition: Lead; Methodology: Equal; Visualization: Equal; Writing – original draft: Equal)

Conflicts of interest

The authors disclose no conflicts.

Funding

This work was supported by National Institutes of Health grants R01 DK48498 (to BME) and P30 CA177558 (to BME). The funding agencies had no role in the study design, collection, analysis, or interpretation of data.